INTERNATIONAL JOURNAL FOR NUMERICAL METHODS IN FLUIDS
Int. J. Numer. Meth. Fluids 2005; **48**:1283–1308
Published online 28 April 2005 in Wiley InterScience (www.interscience.wiley.com). DOI: 10.1002/fld.979

A reference solution for phase change with convection

N. Hannoun[1,*,†], V. Alexiades[1,2,‡] and T. Z. Mai[3,§]

[1]*Department of Mathematics, University of Tennessee, Knoxville, TN 37996-1300, U.S.A.*
[2]*Oak Ridge National Laboratory, Oak Ridge, TN, U.S.A.*
[3]*Mathematics Department, University of Alabama, Box 870350, Tuscaloosa, AL 35487, U.S.A.*

SUMMARY

A reference solutions for phase change involving convection in the melt is currently missing. In the present study, we focus on the problem of melting of pure tin in a square cavity heated from the side, which is used as a benchmark test problem. The mathematical model used for the simulations is based on the enthalpy formulation. Extensive numerical computations are performed with grids as fine as 800×800. The convergence of the numerical solution is demonstrated and its level assessed. Data values and plots are provided for use as a reference solution. Copyright © 2005 John Wiley & Sons, Ltd.

KEY WORDS: benchmark; phase change; pure metal melting; natural convection; enthalpy method; verification

1. INTRODUCTION

The problem of gallium melting in a rectangular cavity heated from the side [1] is frequently used as a comparison exercise in the phase change community. In particular, both the experimental results of Gau and Viskanta [1] and the numerical results of Brent *et al.* [2] are often considered for that purpose. Examples of works referring to these results include References [3–10] where the emphasis is on developing a new numerical method, References [7, 11, 12] for verification purposes, and References [7, 13–15] with interest in the prevailing roll structure in the melt. For a long time the solution of Brent *et al.* was used for comparisons due to its rather good agreement with experimental observation and the lack of a reference solution for the problem. Recently, Hannoun *et al.* [16] have demonstrated

*Correspondence to: Noureddine Hannoun, Department of Mathematics, University of Tennessee, Knoxville, TN 37996-1300, U.S.A.
†E-mail: hannoun@math.utk.edu
‡E-mail: alexiades@utk.edu
§E-mail: tmai@gp.as.ua.edu

Contract/grant sponsor: U.S. Department of Energy; contract/grant number: DE-AC05-00OR22725

Received 14 January 2005
Revised 15 March 2005
Accepted 20 March 2005

what several researchers have argued before [7, 13, 15], that the so-often mentioned solution of Brent *et al.* [2] is actually an incorrect numerical solution due to its inappropriate level of grid convergence.

A problem very similar to gallium melting is the comparison exercise suggested by Gobin and Lequere [17], which involves melting of tin in a square cavity. Contributors to the exercise contrasted their results in References [14, 17] and wide discrepancies were reported. The issue of correct number of cells in the melt was raised for tin melting, as it was for gallium. In Reference [16], the issue was resolved. More recently, Mencinger [18] presented additional results for tin melting showing large discrepancies among various contributors.

Earlier contributors to the problems of tin melting did not assess the accuracy of their numerical solution. In fact, a reference solution for convection phase change seems to be missing in the literature [10, 14–16, 18]. By reference solution, we mean a set of plots and data values (numbers) with known accuracy that one can refer to for comparison purposes. Such a reference solution is needed in view of the unavailability of analytical solutions for convective heat transfer, the mathematical models being too complex. For phase change problems without convection, analytical solutions are available [19, 20].

In the present study, we propose a reference solution for convection phase change problems with accuracy ranging from 0.1 to 1%, depending on the parameter and time considered. This reference solution could be used as a starting problem for verifying a newly developed code.

The present work is organized in two parts. In the first part, we conduct a grid refinement study that demonstrates the convergence level of the numerical solution, while in the second part, we propose a reference solution consisting of a set of plots and data tables. In addition, we clarify some key numerical issues for assessing the accuracy of the tin melting problem.

2. PHYSICAL PROBLEM

The problem considered in the present study was suggested by Lequere *et al.* [17] as a comparison exercise. The configuration is shown in Figure 1. A square cavity is initially filled with pure solid tin at its melting temperature T_f. The right wall is maintained at the same temperature $T_c = T_f$ (no undercooling). At time $t = 0$, the temperature of the left wall is suddenly raised to a temperature $T_h > T_f$ and melting of the solid ensues. Convection in the melt results in several recirculation cells that give the solid–liquid interface a wavy shape. In the present work, we focus on one particular set of values for the dimensionless numbers *Ra* (Rayleigh), *St* (Stefan), and *Pr* (Prandtl). These values as well as other configuration parameters and tin physical properties are shown in Table I.

3. MATHEMATICAL MODEL

For the problem considered, we employ a one-domain enthalpy formulation, which captures fronts without having to track them explicitly. The governing equations are cast in conservative form with Cartesian coordinates and primitive variables (velocity–pressure formulation). The energy equation involves enthalpy, an appropriate choice when phase change is involved. The flow is assumed two-dimensional, unsteady, laminar, and incompressible. The fluid is Newtonian and obeys Fourier's law of heat conduction. The material in the cavity is single

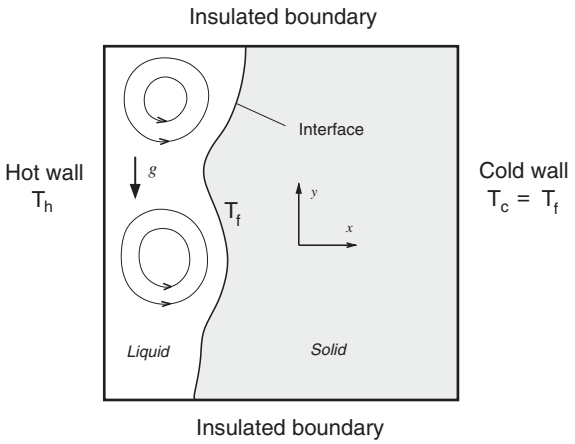

Figure 1. Tin melting problem configuration.

Table I. Tin parameters for the melting problem.

Parameter	Symbol	Tin	Units
Reference density	ρ_{ref}	7.5×10^3	kg/m^3
Specific heat	c_p	200.0	J/kg K
Dynamic viscosity	μ	6×10^{-3}	N s/m^2
Thermal conductivity	κ	60.0	W/m K
Coefficient of volume expansion	β	2.67×10^{-4}	K^{-1}
Latent heat of fusion	L	6×10^4	J/kg
Fusion temperature	T_{f}	505.0	K
Hot wall temperature	T_{h}	508.0	K
Cold wall temperature	T_{c}	505.0	K
Cavity height	H	0.1	m
Cavity width	W	0.1	m
Gravity acceleration	g	10.0	m/s^2
Rayleigh number	Ra	2.5×10^5	
Stefan number	St	0.01	
Prandtl number	Pr	0.02	
Cavity aspect ratio (H/W)	Ar	1.0	

component. Buoyancy effects due to temperature variations are taken into account by invoking Boussinesq's assumption. The thermophysical properties are assumed constant and equal for both solid and liquid phases. The resulting mathematical model, Equations (1), is described by Brent *et al.* [2].

$$\frac{\partial \rho}{\partial t} + \nabla \cdot (\rho \mathbf{V}) = 0 \tag{1a}$$

$$\frac{\partial \rho u}{\partial t} + \nabla \cdot (\rho \mathbf{V} u) = \nabla \cdot (\mu \nabla u) - \frac{\partial P}{\partial x} - Au \tag{1b}$$

$$\frac{\partial \rho v}{\partial t} + \nabla \cdot (\rho \mathbf{V} v) = \nabla \cdot (\mu \nabla v) - \frac{\partial P}{\partial y} - Av + \rho_{\text{ref}}\, g\beta(h - h_{\text{ref}})/c_p \tag{1c}$$

$$\frac{\partial \rho h}{\partial t} + \nabla \cdot (\rho \mathbf{V} h) = \nabla \cdot \left(\frac{\kappa}{c_p} \nabla h\right) - \frac{\partial \rho \Delta H}{\partial t} - \nabla \cdot (\rho \mathbf{V} \Delta H) \tag{1d}$$

Equations (1) are in dimensional form. The source terms in Equations (1b)–(1c) are based on the Carman–Kozeny relation, $A = -C(1 - f_{\text{L}})^2/(f_{\text{L}}^3 + q)$, where C and q are two constants whose values depend on the problem considered. In the mushy zone, $T_{\text{S}} \leqslant T \leqslant T_{\text{L}}$, a linear relationship is assumed between liquid fraction and temperature. The mathematical model is complemented with appropriate initial and boundary conditions. On the boundary, both velocity components are set to zero. The top and bottom boundaries are assumed thermally insulated, while the temperature is specified on the lateral walls. Initially, the material is at rest and at uniform temperature $T = T_{\text{f}}$.

4. NUMERICAL METHOD AND PARAMETERS

The conservation laws, Equations (1) are discretized with a finite-volume method on a uniform Cartesian grid. Space approximations are second order accurate. The convective terms are discretized with the centred scheme. A fully implicit Euler method is employed for time discretization. The resulting nonlinear and coupled system of equations is handled with the SIMPLER algorithm [21]. The sensible, h, and latent, ΔH, heat coupling in the energy Equation (1d) is handled with the procedure described by Brent *et al.* [2]. We use two linear system solvers: BICGSTAB-SIP and CG-SSIP.

To save computational time, all transport equations are solved in a reduced domain containing the liquid. This practice is possible for the energy equation because the solid remains isothermal at temperature T_{f}. In addition, a grid coarsening procedure based on bilinear interpolation is used to transfer data from fine to coarse grids at specified times. The numerical melting range is set as follows: $T_{\text{S}} = T_{\text{f}}$ and $T_{\text{L}} = T_{\text{f}} + \varepsilon$. Note that with this choice of melting range, necessary in view of the lack of undercooling in the benchmark problem and the requirement of the numerical scheme to have a nonzero $T_{\text{f}} - T_{\text{c}} = \varepsilon/2$ interval, $T_{\text{f}} = 505.0125$. Hence, it would be more correct to state that our reference solution is actually for $T_{\text{f}} = 505 + \varepsilon/2$ with undercooling of $\varepsilon/2$ at the right boundary. However, as $\varepsilon \to 0$, both problems should have the same solution.

The simulations are carried out with the following numerical parameter values: $\varepsilon = 0.025$, $\Delta t = 0.1$–0.05 s (decreases as melting proceeds), $C = 10^{15}$, $q = 10^{-6}$, $\omega_{\Delta H} = 0.2$, $\omega_u = \omega_v = 0.7$, $\omega_P = 0.9$, and $\omega_{\text{h}} = 0.8$. Inner iterations (for linear systems) are stopped when a reduction of seven orders of magnitude is achieved for the residual. Outer iterations (during a time step) are stopped when the residual of the conservation equation is less than ε_{o}, where ε_{o} is set to 8×10^{-2}, 10^{-1}, and 10^{-5} for momentum, energy, and mass, respectively. This choice was made after careful inspection of residuals during preliminary simulations.

The code used for the present study has been verified on a series of test problems: the lid driven cavity flow [22], the problem of natural convection in a differentially heated cavity [23], and the problem of melting in a corner [20], all with satisfactory results.

5. RESULTS

5.1. The flow dynamics in the melt

A phenomenological description of the fluid flow in the melt will help to better understand the choice of parameters and plots selected in the present study. The physical problem starts with fully solid tin at its melting temperature in the cavity. Heating of the left boundary to a temperature above the melting point instigates melting. A thin layer of liquid tin forms and convection ensues, due to buoyancy. As melting proceeds, the width of the melt layer increases and the single convection cell keeps growing (Figure 2). Near time $t = 120$ s, a bifurcation occurs, wherein the flow structure suddenly changes to four rolls. Afterwards, both the melt layer and the rolls keep increasing in size. The interface assumes a wave-like shape where the troughs correspond to the roll locations. At some point during the melting process, the rolls get too big to share the cavity. The top two rolls usually merge, thereby decreasing the total number of rolls by one. There are three major roll pairings during the melting process: the first merging occurs around time $t = 210$ s, the second merging close to 480 s, and the third near 1050 s. The third roll merging is not considered in the present work.

5.2. Organization of the results

Selected times for data output are based on the physics of the problem. Five basic times have been selected: (1) $t = 60$ s when the thin melting layer exhibits a single roll, (2) $t = 100$ s when the flow in the melt starts restructuring into a four-roll pattern, (3) $t = 200$ s for the four-roll pattern, (4) $t = 450$ s for the three-roll pattern, and (5) $t = 700$ s for the two-roll pattern. At each selected time, the prevailing structure (number of rolls) is well established

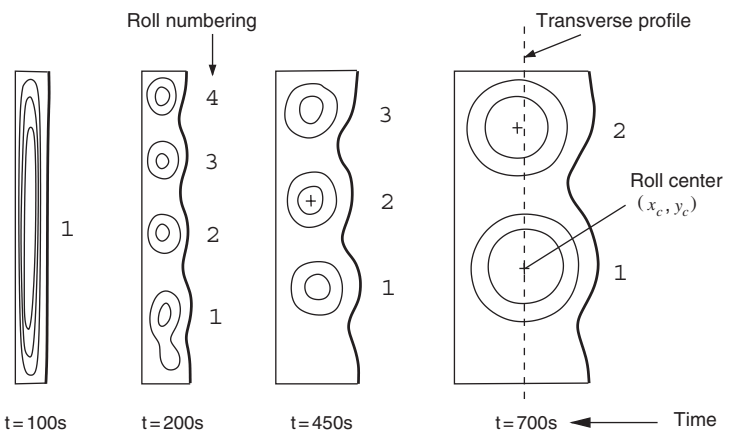

Figure 2. Roll pattern in the melt at several times.

and about to change. The presentation of the results is organized as follows: in the first part, a convergence analysis demonstrates the accuracy of the numerical solution, and in the second part, data values and plots are presented as a reference solution. All the results are given in S.I. units if not otherwise specified.

5.3. *A grid convergence study*

Several parameters are selected to assess the convergence level of the numerical solution. Profiles of streamfunction and temperature as well as roll-centre locations and field values are used as indicators for fluid flow and heat transfer in the melt. Roll-merging and bifurcation times keep track of the time evolution of the flow in the melt. Total liquid fraction in the cavity as well as location of interface crests and troughs are used to monitor both melting process and solid–liquid interface evolution. Last, the Nusselt number at the hot wall is selected for heat transfer rate assessment.

The refinement study carried out in this work is done on a uniform Cartesian grid with sizes ranging from 25×25 to 800×800 nodes. The grid spans the entire cavity in contrast to many other studies where the grid spans the liquid region only. Few nodes are in the liquid early in the melting process, when the liquid layer next to the hot wall is thin. At time $t = 100$ s, for example, the resolution in the melt would be 70×800 for a 800×800 grid. As a result, a fine grid is needed to resolve the thin melt layer at early times. The grid may be coarsened later, when the layer thickness is larger. This is evidenced in Figure 3, which compares the numerical solution at time $t = 450$ s from three different simulations. The first two solutions are from a 400×400 and a 600×600 grids, respectively, while the third solution (called '*600 extrapolated*') is from a mixed grid: 600×600 during time $t = 0$–300 s and 400×400 afterwards. As shown in the figure, coarsening the grid at time 300 s does not affect the accuracy of the solution at time 450 s. In fact, the initial roll location is a determining factor for the accuracy of the roll locations at later times since the rolls keep growing at their initial location. This grid-coarsening procedure reduces considerably the computational resource

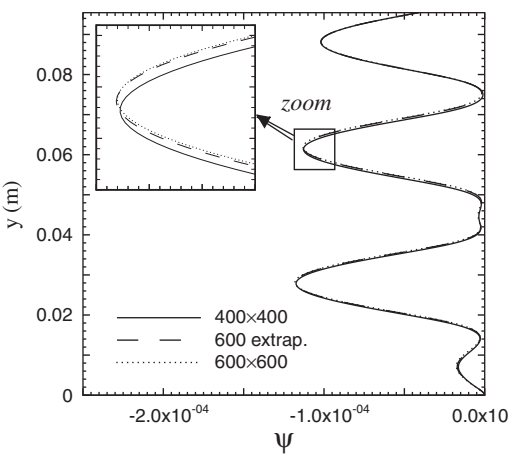

Figure 3. Checking the effect of the restriction procedure at $t = 450$ s.

requirements needed for an entire simulation. Our most accurate solution at time $t = 700$ s will be from a simulation with a 600×600 grid from $t = 0$–300 s, a 500×500 grid from $t = 300$–400 s, and a 400×400 grid afterwards.

5.3.1. Profiles. Transverse profiles of streamfunction and temperature through the centre of the bottom roll (Figure 2) are shown in Figures 4 and 5 at four times. It appears that at time $t = 60$ s, visual convergence is achieved with a 400×400 grid while at time $t = 200$ s, 600×600 nodes are required for the same purpose. As may be noticed on the plots, the main accuracy issue is one related to the vertical location of the rolls.

There is a slight discrepancy (vertical shift) between the finest two grid solutions at time $t = 450$ s. There is no 800×800 grid result available to assess the accuracy of the 600×600 grid solution. However, as indicated by the $t = 200$ s plot, the 600×600 grid is fine enough to capture the correct early roll locations. In view of the fact that the grid does not need refinement (actually may be coarsened) after time 200 s (see the discussion in Section 5.3), we believe the 600×600 grid solution to have the same accuracy at times 450 and 200 s. At time $t = 700$ s, the most accurate solution '600 extrapolated' (see Section 5.3) differs only slightly from the 400×400 solution.

5.3.2. Roll-centre parameters. The transient for the tin melting problem is very sensitive to the roll locations in the melt. In particular, the roll-merging times, the shape of the solid–liquid interface, and the Nusselt number Nu are strongly affected by the initial roll locations. Hence, it is very important to capture the rolls accurately. Figure 6 displays the effect of grid refinement on the roll-centre location y_c and streamfunction value ψ_c at time $t = 200$ s (see Figure 2 for roll numbering and associated nomenclature). As may be noticed, there is a good convergence pattern. Similar results, not shown here, are obtained for times 450 and 700 s.

A quantitative estimate of the convergence level is provided in Table II, which displays the values obtained for the finest two grids as well as an extrapolated value based on Richardson's extrapolation. The relative error for the finest grid solution is then computed assuming the extrapolated value is the exact value. The errors so calculated are seen to lie between 0.1% and 0.96% with the largest error corresponding to the location of Roll#2 at times $t = 200$ and 450 s. Elsewhere, the error does not exceed 0.5%.

5.3.3. Interface location and total liquid fraction. With the enthalpy method, the solid–liquid interface is usually defined as the $f_L = 0.5$ contour line. Here we adopt a slightly different definition: for a given y value, the solid–liquid interface location, x_{int}, is defined as the width of the equivalent liquid content of the corresponding row of fluid, i.e. if all the liquid at height y is pilled up to the left, the liquid would have width equal to x_{int}. The interface so obtained is almost indistinguishable from the $f_L = 0.5$ contour curve.

Figure 7 displays the solid–liquid interface obtained with several grids. For clarity, only the grids essential for demonstrating the convergence of the solution are shown. The interfaces obtained with the 400×400 and the 300×300 grids are almost indistinguishable. Clearly, interface location converges faster than other variables such as ψ. At time 100 s, the interface is flat since only one cell is present in the liquid.

Convergence of the interface location is slower at the troughs and crests along the interface. Figure 8 shows the effect of grid refinement for the troughs, the crests, and the top and bottom

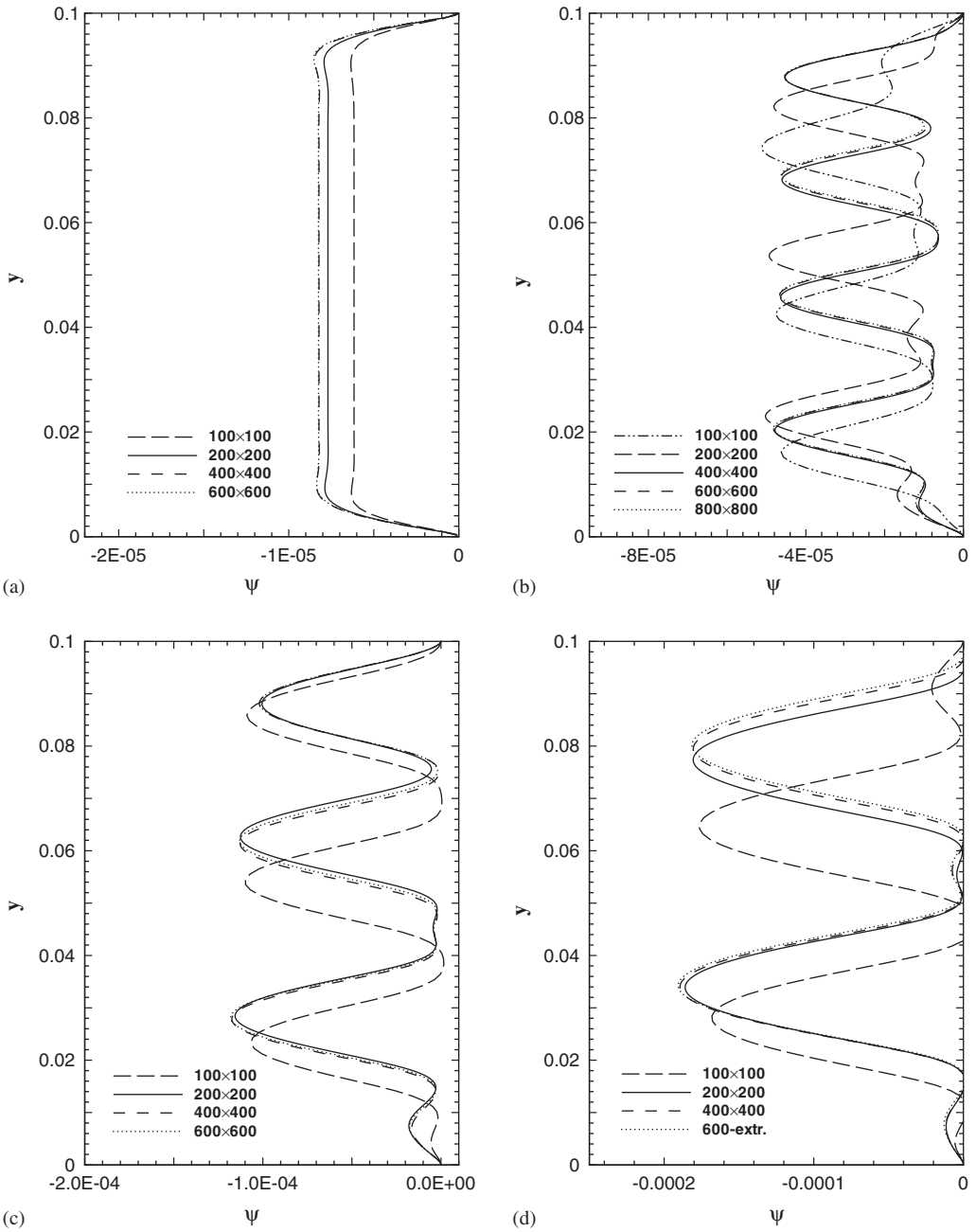

Figure 4. Grid convergence of streamfunction transversal profiles at four times: (a) $t = 60$ s, $x = 0.003417$; (b) $t = 200$ s, $x = 0.0063$; (c) $t = 450$ s, $x = 0.01006$; and (d) $t = 700$ s, $x = 0.01346$.

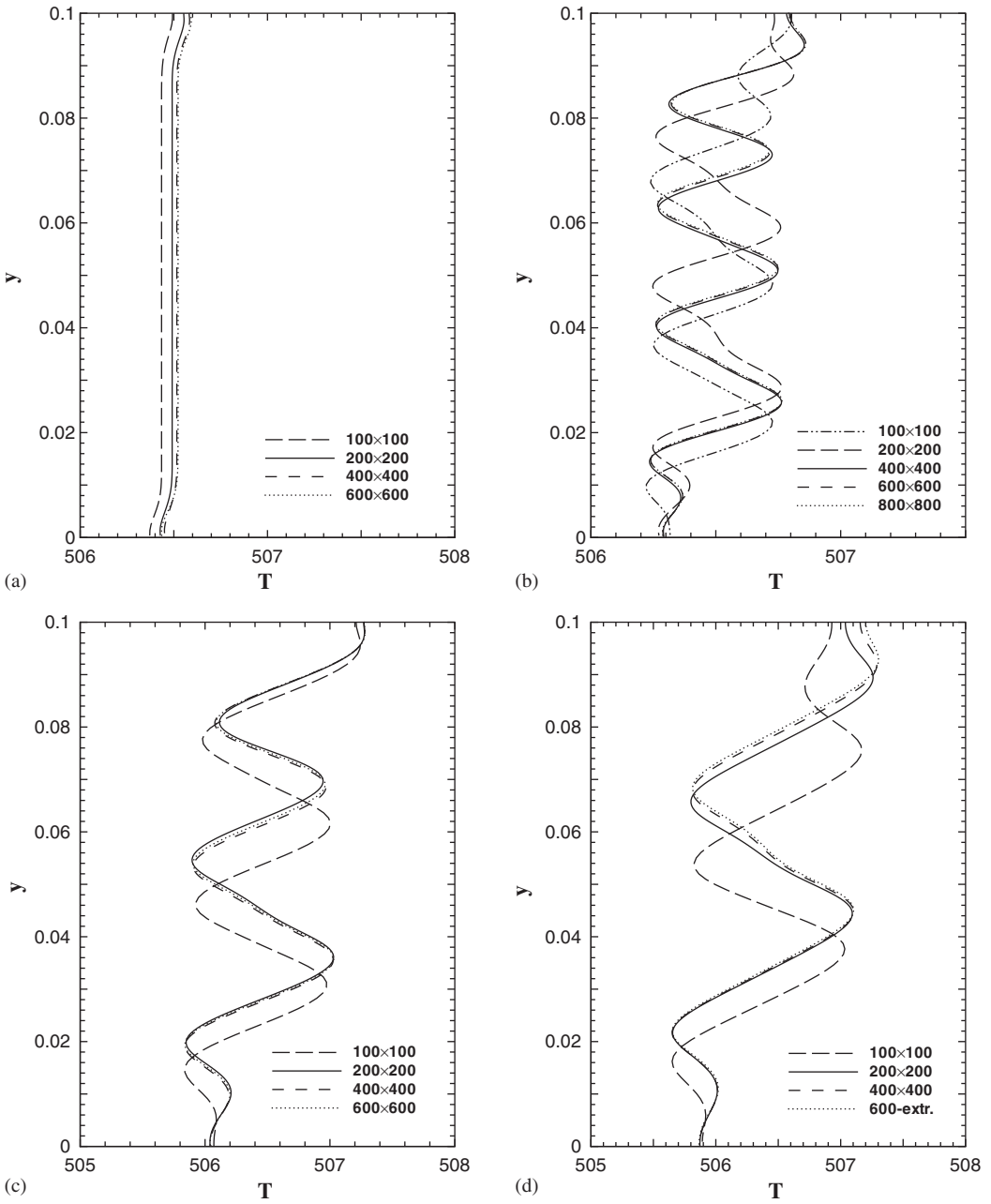

Figure 5. Grid convergence of temperature transversal profiles at four times: (a) $t = 60$ s, $x = 0.003417$; (b) $t = 200$ s, $x = 0.0063$; (c) $t = 450$ s, $x = 0.01006$; and (d) $t = 700$ s, $x = 0.01346$.

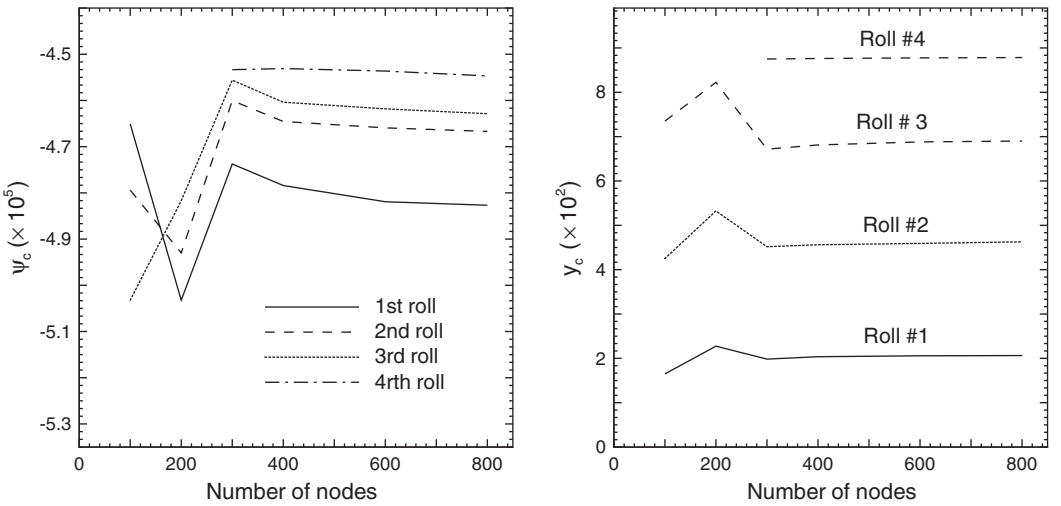

Figure 6. Effect of grid refinement on roll parameters at times 200 s.

Table II. Extrapolated values of the roll-centre location (y-coordinate) and the corresponding streamfunction value.

		Time 200 s				Time 450 s			
	Roll	Mesh 1/600	Mesh 1/800	Extrap.	Err. (%)	Mesh 1/400	Mesh 1/600	Extrap.	Err. (%)
y_c	#1	0.02058	0.02063	0.02069	0.31	0.02787	0.02792	0.02796	0.14
	#2	0.04592	0.04627	0.04672	0.96	0.06137	0.06192	0.06236	0.70
	#3	0.06880	0.06900	0.06926	0.37	0.08787	0.08825	0.08855	0.34
	#4	0.08775	0.08783	0.08793	0.11				
$-\psi_c \times 10^4$	#1	0.48192	0.48268	0.48366	0.20	1.174	1.180	1.185	0.40
	#2	0.46594	0.46670	0.46767	0.20	1.128	1.130	1.132	0.14
	#3	0.46182	0.46287	0.46422	0.29	1.018	1.0184	1.01872	0.31
	#4	0.45364	0.45469	0.45604	0.30				

points of the interface at time $t = 450$ s. The y-locations of the crests and troughs are from the finest grid solution.

The actual error on the calculated interface location, $\max |(x_e - x_{int})/x_e|$, where x_e is a value obtained from Richardson's extrapolation, is shown at three times in Table III. However, x_e being small exaggerates the value of the relative error. Normalizing by the cavity width W, the error does not exceed 0.3%. Notice that the error is largest at time $t = 700$ s. This is to be expected since the error estimate is from the 300×300 and 400×400 grids, Richardson's extrapolation precluding the use of a hybrid grid such as the one used for the finest available solution, the 600-extrapolated solution. Therefore, the calculated error might very well overestimate the actual error. Indeed, if the error is computed as the difference between the finest

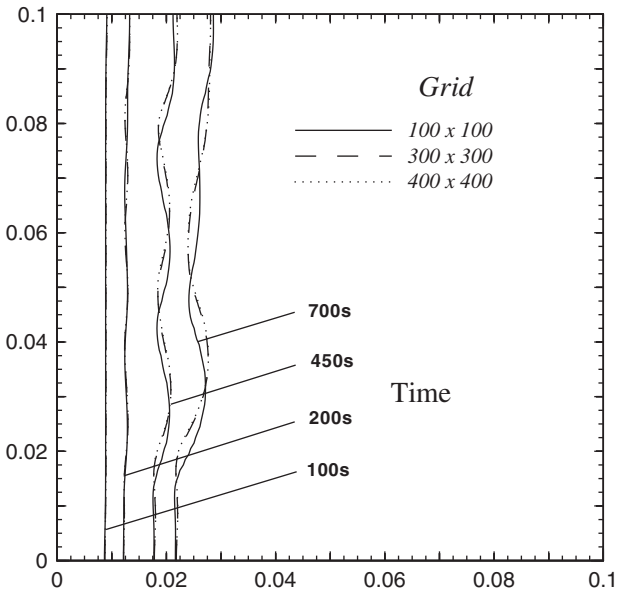

Figure 7. Grid convergence of interface at several times.

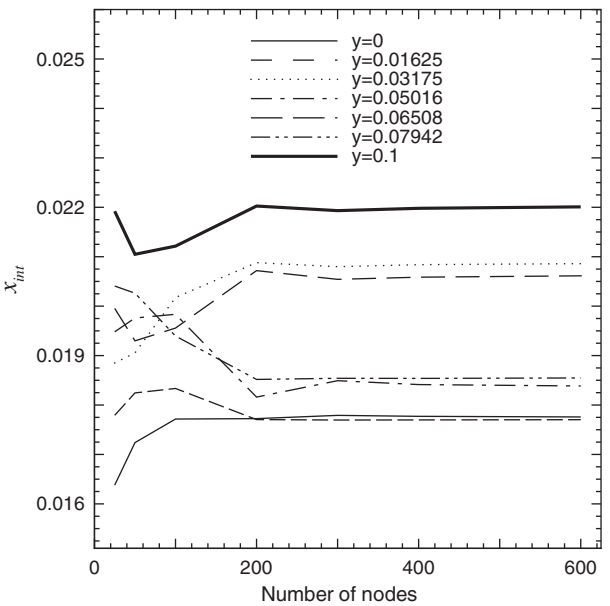

Figure 8. Grid convergence of trough and crest locations at time $t = 450$ s.

Table III. Error on the calculated solid–liquid interface location.

	Time t(s)			
	Richardson's		700	
	200	450	Richardson's 300×300 and 400×400 grids	$\lvert x_{600\text{ext}} - x_{400} \rvert$ Finest grids
Error (%)	0.18	0.62	1.07	0.4
Error/W	0.02	0.13	0.30	0.1

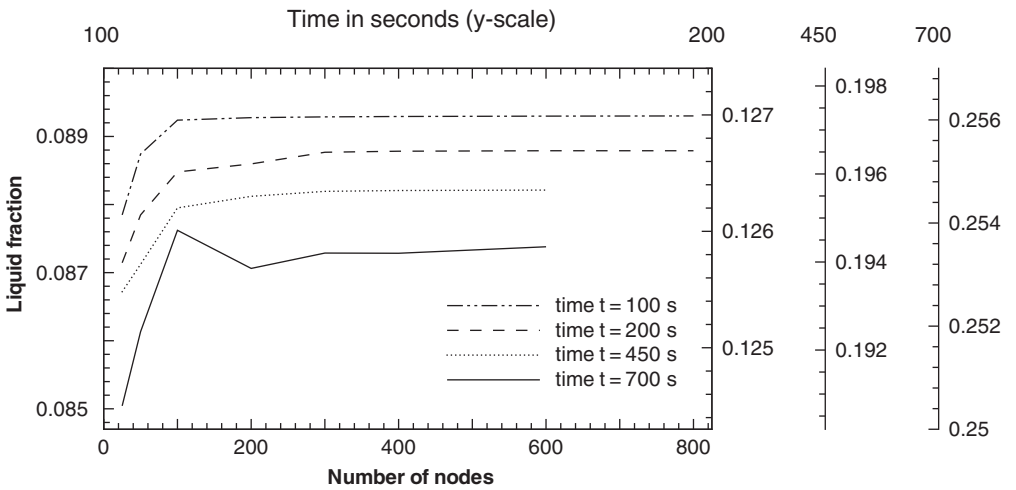

Figure 9. Grid convergence of total liquid fraction in the cavity at several times.

two grid solutions (600-extrapolated and 400×400 grid solutions), the relative error drops to 0.4% and the error normalized by the width W to 0.1% as shown in the last column of Table III.

The liquid fraction, ratio of melted tin and cavity volumes, is often used for comparison purposes in the literature. Figure 9 displays the convergence of the total liquid fraction with grid refinement at four times. Each curve has its own y-axis to allow for the representation on a single graph.

Richardsons's extrapolation procedure is used to obtain a better approximation of the total liquid fraction value, which in turn is used to calculate the error of the approximation on each grid. A log–log plot of the relative error as a function of the normalized mesh spacing is shown in Figure 10. The slope of the curves obtained is close to two, the order of space discretization. The error on the liquid fraction is less than 0.05% for all four times.

5.3.4. Roll-merging and bifurcation times. The melting process for the problem under study involves several major transition times: the time for onset of four-roll pattern as well as three roll-merging times (see Section 5.1). Assigning a value to these critical times is not trivial

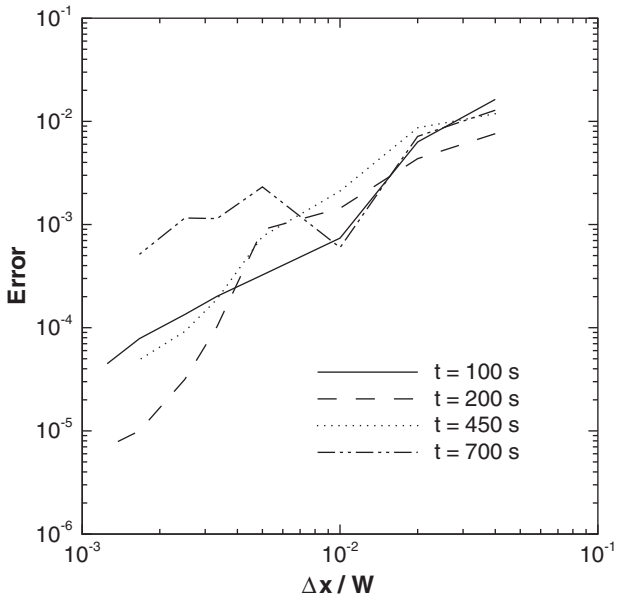

Figure 10. Error convergence with grid refinement of total liquid fraction in the cavity.

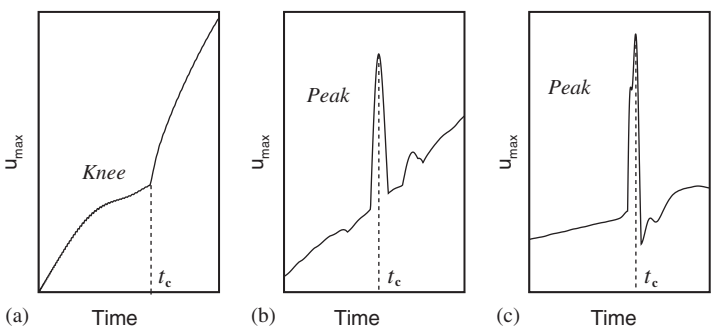

Figure 11. Definition of the critical times t_c for roll mergings and bifurcations with the u_{max} versus time plot: (a) onset of four rolls; (b) 1st roll merging; and (c) 2nd roll merging.

because the roll mergings as well as the onset of four-roll pattern are continuous processes. Inspection of the time evolution of several flow quantities reveals that some parameters are very sensitive to the transitions. For example, the onset of four-roll pattern results in a sudden slope change of the u_{max} versus time plot (Figure 11(a)), which exhibits a knee at that particular time. The parameter u_{max} stands for the maximum value of the u velocity component over the entire flow field. For the roll mergings, other parameters may be used, e.g. ψ_{min}, the minimum ψ field value, and u_{var}, the integral over the computational domain of the absolute value of u change in one time step. However, u_{max} also reveals them well: a peak appears on the graph near the transition time (Figure 11(b) and 11(c)) and the highest point on the peak is selected for evaluating the merging time t_c.

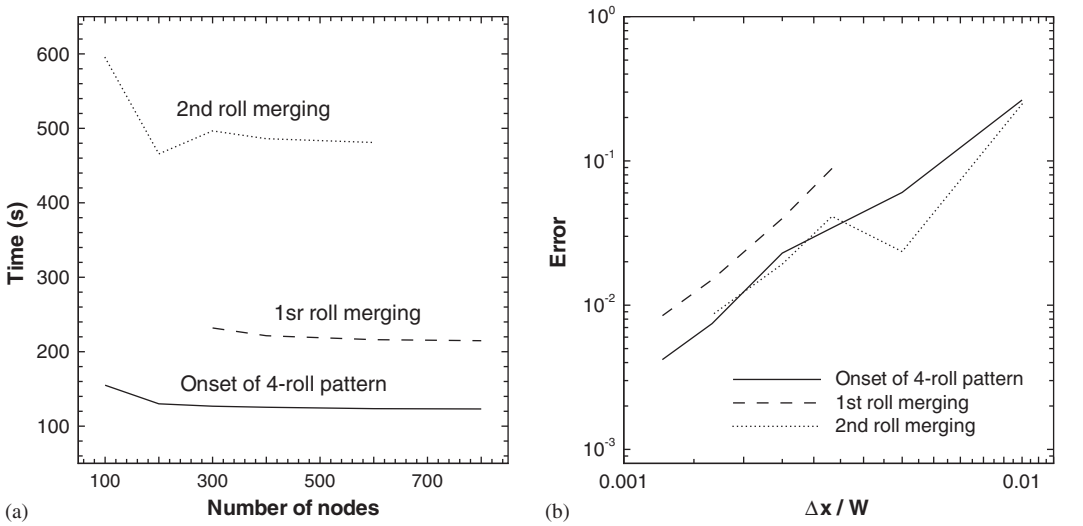

Figure 12. Effect of grid refinement on the transition time approximations: (a) transition time; and (b) relative error.

Figure 12 displays the effect of grid refinement on three transition times: onset of four-roll pattern, first roll-merging, and second roll-merging times. Clearly, convergence is monotone as shown in Figure 12(a). Richardson's extrapolation is used to obtain better approximations and the corresponding relative errors are plotted in Figure 12(b) versus mesh spacing, normalized by the width (also height) of the cavity. Second order convergence is observed for all plots (slope is close to 2). The maximum estimated error is close to 0.3% for the onset of four-roll pattern and less than 0.8% for the two roll mergings.

5.3.5. Nusselt number plots. The average Nusselt number Nu at the hot wall measures the heat transfer rate through the cavity. Nu is defined as the ratio of the actual heat flux through the wall and the heat flux that would prevail without convection (pure conduction). Figure 13 displays Nu versus time for grid sizes up to 600×600. To make the graph more readable, consecutive curves are shifted 2 units vertically from one another. There is very good agreement between the finest two grid (400×400 and 600×600) solutions. Only a minor shift of the drop may be noticed. This sudden drop, near time $t = 480$ s, corresponds to the second roll merging. Notice the very good agreement between the 600×600 and the 600-extrapolated merging times, confirming the appropriateness of the grid coarsening procedure.

5.4. Time step considerations

The results presented in the previous sections focused primarily on the effect of grid refinement. Since the problem being studied is unsteady, it is necessary to assess the adequacy of the time step choice. Several time step values have been tested after a basic value was calculated from the classical CFL condition. When further refinement did not lead to significant changes (usually up to the fourth digit), the time step was considered small enough.

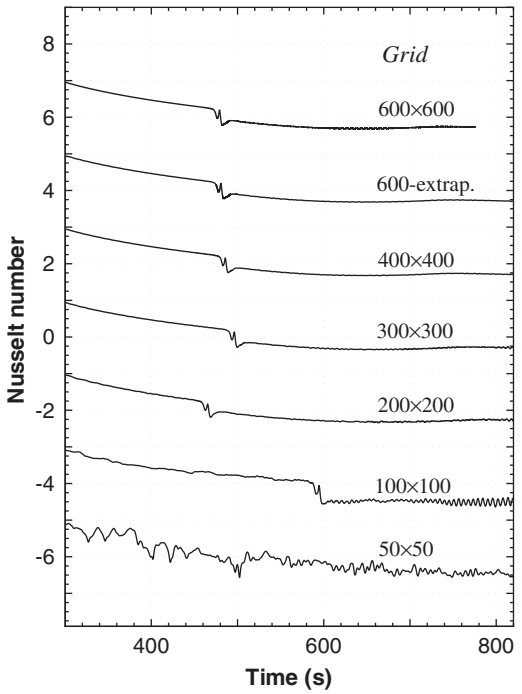

Figure 13. Grid convergence of average Nusselt number at the hot wall. Plots are shifted 2 units vertically. y-scale is for the top plot.

In particular, a time step ten times smaller than the one employed in the present calculations has been used to check the accuracy of the solution at high transients (roll mergings).

5.5. *A reference solution*

Having demonstrated the convergence of the numerical solution under grid refinement, we present selected values and plots for use as a reference solution. The values are from the most accurate grid, except for the transition times, which are obtained through Richardson's extrapolation. Hence, the 800×800 grid solution is used for times 0–225 s, the 600×600 solution for times 225–500 s, and the 500×500 grid solution, restricted from the 600×600 solution at time 500 s, is used afterwards. All variables are dimensional, and in S.I. units if unspecified.

We provide data tables for transverse profiles (Table IV), interface location (Table V), time evolution of Nusselt number, total liquid fraction and flow field extreme values (Table VI), transition times (Table VII), and roll-centre parameters (Tables VIII–X). Plots are provided for the time evolution of $\psi_{\min}$ and $u_{\max}$ values (Figure 14), the Nusselt number and total liquid fraction (Figure 15), and flow parameters at two carefully selected monitoring points shown in Figures 16 and 17.

The max error is estimated to be 0.96% for the roll-centre locations, 0.4% for the roll-centre field values, 0.6% for the interface, 0.1% for the total liquid fraction, and 0.8% for the roll-merging and bifurcation times.

Table IV. Transverse profiles of streamfunction ψ and temperature T at three times.

	Time 200 s $x = 0.0063$		Time 450 s $x = 0.01006$		Time 700 s $x = 0.01346$	
y (m)	$\psi \times 10^5$	T (K)	$\psi \times 10^4$	T (K)	$\psi \times 10^4$	T (K)
0.000	0.00000	506.289	0.00000	506.041	0.00000	505.866
0.005	−1.13147	506.335	−0.14870	506.100	−0.10255	505.916
0.010	−1.01166	506.346	−0.13151	506.199	−0.10869	506.015
0.015	−2.50584	506.239	−0.03275	506.026	−0.00094	505.937
0.020	−4.78860	506.463	−0.44922	506.843	−0.14267	505.691
0.025	−3.22922	506.752	−1.05104	506.156	−0.96751	505.741
0.030	−0.84784	506.648	−1.13372	506.676	−1.69568	506.099
0.035	−0.77794	506.453	−0.61249	507.021	−1.89963	506.504
0.040	−1.90118	506.267	−0.06117	506.823	−1.52562	506.89
0.045	−4.51424	506.484	−0.04083	506.441	−0.68837	507.103
0.050	−3.43867	506.726	−0.05067	506.082	−0.04424	506.851
0.055	−0.83490	506.638	−0.56915	505.918	−0.06975	506.486
0.060	−0.78910	506.378	−1.08227	506.276	−0.02925	506.255
0.065	−3.26631	506.286	−0.99995	506.770	−0.07892	505.929
0.070	−4.53440	506.573	−0.39213	506.947	−0.78321	505.841
0.075	−2.03444	506.695	−0.01980	506.524	−1.53069	506.145
0.080	−1.20603	506.413	−0.31777	506.101	−1.81390	506.548
0.085	−3.82606	506.378	−0.88847	506.306	−1.55184	506.942
0.090	−4.08494	506.720	−0.97383	506.828	−0.80850	507.246
0.095	−1.09192	506.854	−0.47331	507.221	−0.08628	507.278
0.100	0.00000	506.792	0.00000	507.275	0.00000	507.201

6. DISCUSSION

6.1. *On the mathematical model*

There are two main approaches to macroscopic modelling of phase change problems, front-tracking and front-capturing [19]. In the older, classical, front-tracking approach, the conservation laws are imposed in each phase separately and explicit interface conditions must be imposed to ensure conservation across phases, which provide the additional equations necessary to determine the unknown moving boundary, as in the classical Stefan problem. This, of course, assumes *a priori* that the interface is a smooth mathematical surface, and cannot be applied to complicated problems.

The alternative, front-capturing, one-domain approach, makes no *a priori* assumptions about structure and smoothness of fronts, by posing the conservation laws globally, irrespective of phase. Interface conditions are obeyed automatically as 'natural boundary conditions' (in the sense of calculus of variations), are not explicitly stated or enforced. The thickness of the phase transition (mushy) region results from the solution and not dictated *a priori*; its location can be recovered from the solution *a posteriori*. This, enthalpy formulation (similar to shock capturing in gas dynamics), is the most viable general approach, valid for simple and complicated problems alike.

Table V. Interface location $x_{\text{int}}(m)$ as a function of height y at four times.

	Time (s)			
y (m)	100	200	450	700
0.000	0.008749	0.01215	0.01776	0.02180
0.005	0.008796	0.01225	0.01793	0.02199
0.010	0.008868	0.01231	0.01802	0.02211
0.015	0.008915	0.01227	0.01774	0.02186
0.020	0.008932	0.01264	0.01822	0.02215
0.025	0.008929	0.01297	0.01986	0.02450
0.030	0.008927	0.01283	0.02079	0.02657
0.035	0.008929	0.01254	0.02065	0.02761
0.040	0.008929	0.01235	0.01973	0.02762
0.045	0.008929	0.01268	0.01882	0.02667
0.050	0.008929	0.01294	0.01838	0.02510
0.055	0.008929	0.01274	0.01901	0.02408
0.060	0.008929	0.01243	0.02015	0.02396
0.065	0.008928	0.01253	0.02060	0.02435
0.070	0.008929	0.01289	0.02017	0.02540
0.075	0.008932	0.01282	0.01917	0.02663
0.080	0.008926	0.01247	0.01856	0.02752
0.085	0.008927	0.01260	0.01999	0.02794
0.090	0.008982	0.01311	0.02149	0.02804
0.095	0.009087	0.01328	0.02204	0.02809
0.100	0.009142	0.01327	0.02201	0.02812

Table VI. Nusselt number, liquid fraction, and maximum and minimum field values for velocity components and streamfunction.

	Time (s)							
	100	200	300	400	450	500	600	700
Liq. fraction	0.08930	0.12670	0.1563	0.1829	0.1956	0.2077	0.2309	0.2536
Nu	11.25220	8.15200	6.9560	6.4660	6.3000	5.8930	5.7040	5.7120
$\psi_{\max} \times 10^6$	0.00351	0.00476	0.1472	0.5739	0.8907	1.2809	1.4500	1.9550
$\psi_{\min} \times 10^4$	−0.19710	−0.48827	−0.7650	−1.0420	−1.1810	1.3530	−1.6290	−1.9060
$u_{\max}$ (m/s)	0.00240	0.00685	0.0104	0.0132	0.0143	0.0156	0.0172	0.0186
$u_{\min}$ (m/s)	−0.00237	−0.00645	−0.0101	−0.0129	−0.0141	−0.0154	−0.0171	−0.0187
$v_{\max}$ (m/s)	0.00699	0.01205	0.0149	0.0170	0.0179	0.0193	0.0207	0.0222
$v_{\min}$ (m/s)	−0.00708	−0.01179	−0.0143	−0.0163	−0.0171	−0.0192	−0.0198	−0.0211

It is based on the weak formulation (see Reference [19]) of conservation laws, which constitutes a well-posed mathematical problem (admits unique, stable solution), and it has been established mathematically that it reduces to the sharp interface limit whenever the latter exists. In that case, the numerical solution also converges to the sharp interface solution as $\Delta x, \Delta t \to 0$. Newer developments in this spirit include phase-field formulations, and level set methods for evolving fronts.

Table VII. Bifurcation and roll-merging times.

	Time (s)
Onset of four-roll pattern	122.6
First roll merging (4 to 3 rolls)	213.0
Second roll merging (3 to 2 rolls)	490.2

Table VIII. Parameters of the four rolls at time 200 s.

Roll	1	2	3	4
x_c (m)	0.00631	0.006322	0.0066311	0.006443
y_c (m)	0.02063	0.04627	0.06900	0.08783
$\psi_c \times 10^5$	−4.82682	−4.66698	−4.62875	−4.54689
T_c (K)	506.507	506.508	506.505	506.531

Table IX. Parameters of the three rolls at time 450 s.

Roll	1	2	3
x_c (m)	0.009917	0.009917	0.01025
y_c (m)	0.02792	0.06192	0.08825
$\psi_c \times 10^4$	−1.18	−1.12989	−1.01841
T_c (K)	506.47	506.484	506.628

Table X. Parameters of the two rolls at time 700 s.

Roll	1	2
x_c (m)	0.0134582	0.0136101
y_c (m)	0.0342582	0.0801195
$\psi_c \times 10^4$	−1.90609	−1.81429
T_c (K)	506.44	506.557

The enthalpy method for phase change problems is very popular due to its inherent conceptual advantages, its simplicity, efficiency, generality, and robustness. It has been shown to produce results in good agreement with other numerical techniques, such as front-tracking with adaptive mesh [24].

Although newer methods, such as the immersed boundary method [25], the sharp interface method [26], and the phase field method [27] have been suggested as improvements over the enthalpy method, they were designed for finer (mesoscopic) scale phenomena, such as problems involving surface tension and dendritic solidification, mostly without flow, and results are still mostly qualitative. Both the immersed boundary and phase field methods are in fact enthalpy-type, with the interface spread over at least one control volume.

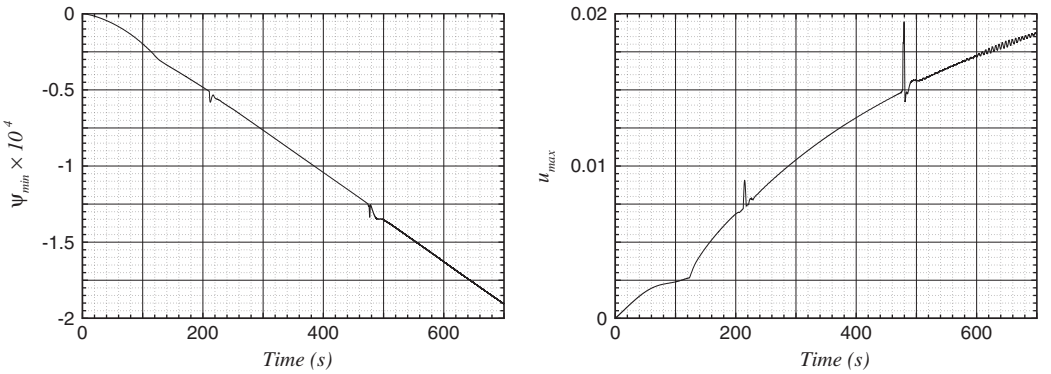

Figure 14. Time evolution of min streamfunction and max u velocity component values.

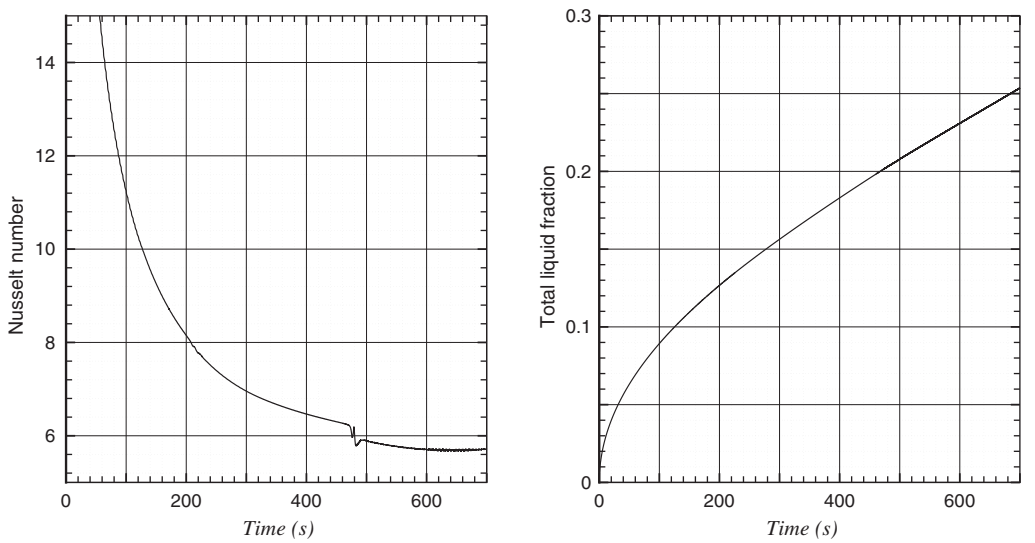

Figure 15. Time evolution of the total liquid fraction in the cavity as well as the average Nusselt number at the hot wall.

For a macroscopic description of melting, it is arguable whether an idealized sharp interface (as in the Stefan problem) is physically more correct than a mushy zone allowed by the enthalpy formulation. After all, a physical interface is not really a mathematically sharp surface. Ultimately, this is an issue of model validation against experimental data, which is exceedingly hard to carry out (see Reference [16]), and as far as we know, it is still open for the gallium and tin melting problems.

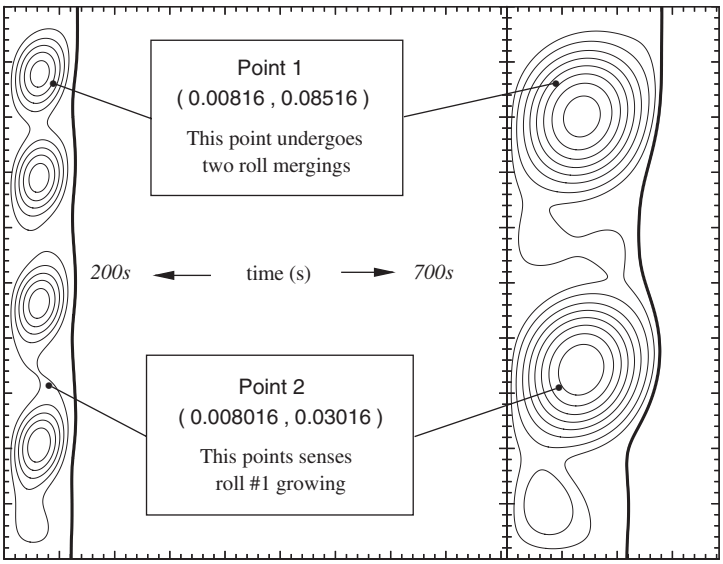

Figure 16. Location of the points where time evolution of parameter values are recorded.

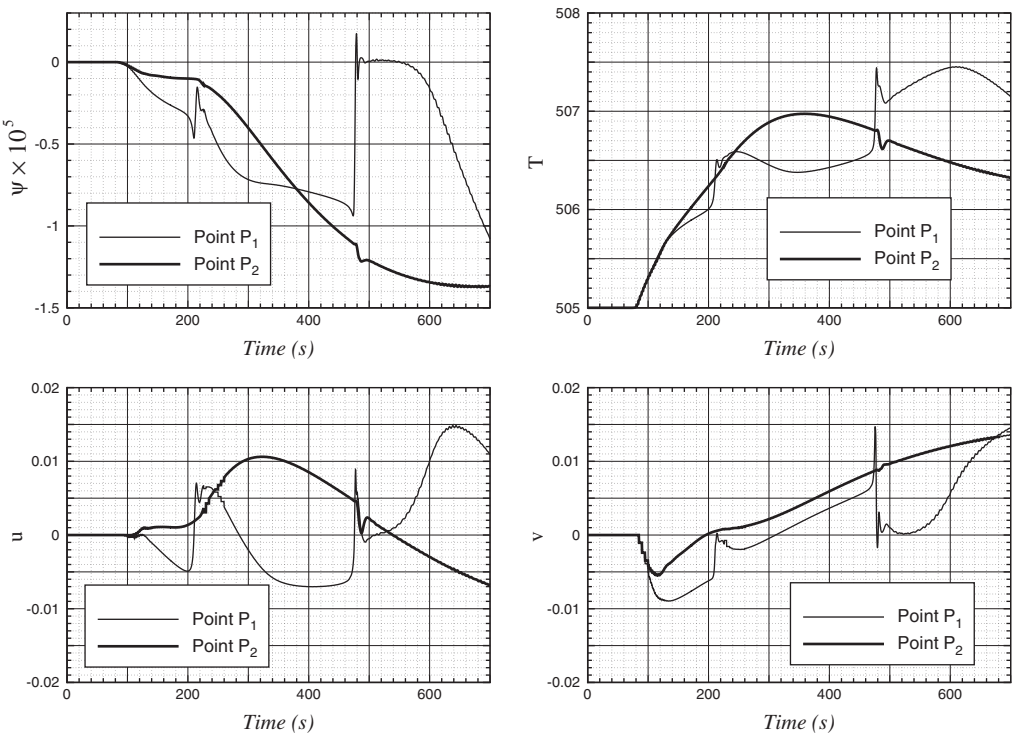

Figure 17. Time evolution of streamfunction ψ, temperature T, and velocity components u and v at two points, $P_1(0.00816, 0.08516)$ and $P_2(0.008016, 0.03016)$.

6.2. On the numerical method

The present work aims at providing a much needed reference solution for phase change with convection, employing the most commonly used formulation and standard, well-understood numerical methods. Our control volume centred discretization, being of order 2 in space and 1 in time, is probably not the most efficient numerical technique today. However, this discretization is robust and reliable. It does not involve additional error sources due to extraneous procedures such as interpolation/extrapolation needed after mesh adaptation or flux correction needed to ensure monotonicity of higher order schemes.

Given that the mathematical model is well-posed, any convergent (consistent and stable) numerical method will produce an approximation that ultimately converges to the unique solution of the model. Lower order methods are certainly slower to converge (require finer mesh). In the present study, the numerical method was pushed to its limits and we managed to reach time $t = 700$ s. Beyond that, adaptive mesh refinement, higher order schemes, and parallelization may be necessary to reach an acceptable convergence level.

6.3. A crucial issue

The grid refinement study carried out in this work shows, among other things, that a crucial issue in the simulation of the tin melting problem is whether or not the roll locations, early in the melting process (around $t = 200$ s), are predicted accurately. The actual cell structure in the melt has been reported in many publications (reviewed and discussed in Reference [16]) but the accuracy of the roll locations as well as the values of streamfunction and temperature at the roll centres had not been addressed. A small error in the actual roll location changes dramatically the times for roll mergings. This can be observed in Mencinger's results (Reference [18], Figure 12(d), p. 260) which shows how the drop in the $Nu(t)$ plot shifts to the right when the grid is refined. In fact, our results indicate a time for the third roll merging close to 1050 s, in contrast to 1000 s ($\Delta Fo = 4$) suggested in Mencinger's results (a 5% discrepancy). This result is actually consistent with our observations, that a decrease in resolution (either grid size or discretization scheme order) usually results in an earlier roll pairing. When the resolution is lower, the top two rolls are closer (incorrect location), and they merge faster.

6.4. Enough nodes or not enough

Recently, Mencinger [18] presented additional results on the tin melting problem. In his work, he indicates that with his method, in contrast to other numerical results [15, 16], even a coarse grid '40×40' captures well the physical behaviour of the system such as the flow instabilities (roll merging). However, his results (Figure 12(d), p. 260) show a 25% error for the second roll-merging time obtained with the 40×40 grid. This is a strong indication that the roll structure is not accurately resolved early in the melting process. If his intended meaning is that several rolls may be captured with a 40×40 grid, then several rolls were also obtained with a 50×50 grid in Reference [16] with the second order centred scheme. But that does not mean such coarse solutions are correct (converged). His conclusion, that the origin of the discrepancies of contributed solutions in comparison exercise #1 [14, 17] could simply be insufficient grid density for the specified cases, was already suggested in many earlier works [7, 13, 15] and clearly demonstrated for the case of tin melting in Reference [16].

6.5. *The oscillatory nature of the solution*

An interesting feature shown in Figure 13 is the presence of oscillations on the *Nu* plot for the coarse grids after time $t = 500$ s (i.e. the second roll-merging). Oscillations of the *Nu* plot were reported in three publications [10, 14, 18]. Wintruff *et al.* [10] add that these oscillations are generated by pulsations of the rolls in the melt. Mencinger [18], who acknowledges the possibility of purely numerical oscillations, suggests that the observed oscillations are actually physical. He adds that the time step Δt should be small enough ($\leqslant 0.01$ s) in order to capture the physical oscillations. Our results indicate that oscillations may show up even for a larger time step $\Delta t = 0.1$ s (Figure 13, grids 50×50 and 100×100). Reducing the time step by a factor 10 does not affect the solution. Moreover, the oscillations seem to fade away as the grid is refined from 50×50 to 400×400 (Figure 13), which seems to indicate that the oscillations are of numerical origin. Inspection of the Nusselt number plots at a later time, Figure 18, confirms that trend. A possible explanation for theses oscillations is the fact that the cell Peclet number for the simulations is too large. In our simulations, $Pe > 2$ when $t > 500$ s even with the finest grid. This is one of the reasons we do not present results beyond time $t = 700$ s. The coarse grid used by Mencinger may well correspond to a cell Peclet number of the order of $Pe = 30$. Further work may be needed in order to resolve this issue.

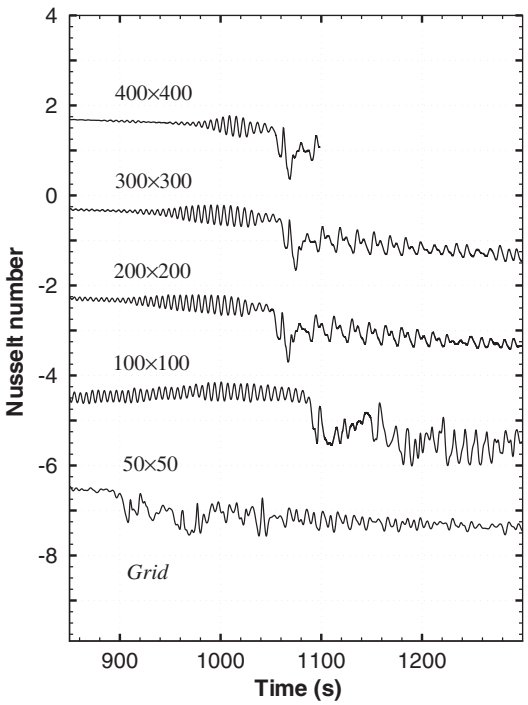

Figure 18. Grid convergence of average Nusselt number at the hot wall. Plots are shifted 2 units vertically. *y*-scale is for the top plot.

Table XI. CPU requirements for several simulations.

Grid	Time (s)	CPU (h)	Machine
100×100	0–700	20	SUN Enterprise 6000
200×200	0–700	260	CRAY SV1
400×400	0–700	450	Compaq Alpha ES40
600-extrap.	0–700	1070	Compaq Alpha ES40
600×600	0–500	2500	Compaq Alpha ES40
800×800	0–225	1750	Compaq Alpha ES40

6.6. On the accuracy of the reference solution

In many earlier benchmark solutions, the accuracy achieved was close to 0.1% or better. Some of our results are not as accurate, and as a consequence, it is legitimate to question the use of the term 'Reference Solution'. Earlier benchmark problems were mostly for steady state problems, or involved only one primary length scale. Even today, phase change problems coupled to convection are highly demanding in computational resources. As a result, there has not been any reference solution published to date [14, 15, 17]. Earlier publications about the tin or gallium melting problems mostly focused on global solution features, and a 10% agreement between two distinct solutions for the same problem was often considered satisfactory (see for example Reference [28]). In the present study, we provide the first thoroughly documented data values for a phase change problem involving convection in the melt. Many of our results are accurate to within 0.1% and some only to within 1%. Further improvements via higher order schemes and/or adaptive mesh refinement are to be considered.

6.7. Computational resources

The CPU requirements for some of the simulations are presented in Table XI. Some of the simulations took months to complete. Parallelization is an option to consider for carrying out such demanding computations.

7. CONCLUSION

The lack of a reference solution for phase change problems involving convection in the melt is a current issue that needs to be resolved. In this work, we present a convergence study for the problem of tin melting in a vertical cavity heated from the side. The mathematical model selected for this benchmark problem is based on the enthalpy formulation. Grid refinement plots are provided for most physical quantities of interest, demonstrating a good level of convergence. The physical processes involved in the tin melting problem are also documented. The reference solution includes tables of values as well as various plots for the most important features of interest. The accuracy achieved in this work is as good as 0.1% for many parameters, with some only accurate to within 0.96%. This work provides the research community with a thoroughly documented reference solution that can be used as a starting point to verify other codes and models and also for further investigations on the same problem.

NOMENCLATURE

Letters

A	porosity constant
c_p	specific heat
C	porosity constant
f_{L}	liquid fraction
g	gravity acceleration
h	sensible enthalpy (c_pT)
H	cavity height
L	latent heat of fusion
Nu	Nusselt number ($Q_{\mathrm{w}}/Q_{\mathrm{c}}$)
P	pressure
Pr	Prandtl number (v/α)
q	porosity constant
Q_{c}	wall heat flux without convection
Q_{w}	wall heat flux with convection
Ra	Rayleigh num.: $g\beta(T_{\mathrm{h}} - T_{\mathrm{f}})H^3/\alpha v$
St	Stefan number $c_p(T_{\mathrm{h}} - T_{\mathrm{c}})/L$
t	time
T	temperature
u	x-velocity component
v	y-velocity component
$\mathbf{V}$	velocity vector
W	cavity width
x_{int}	interface location
x, y	Cartesian coordinates

Greek letters

α	thermal diffusivity ($\kappa/\rho c_p$)
β	coefficient of thermal expansion
ΔH	latent enthalpy content ($f_{\mathrm{L}}L$)
ε	numerical solidification T range
ε_{o}	outer iterations convergence tolerance
κ	thermal conductivity
μ	dynamic viscosity
ν	kinematic viscosity
ρ	density
ψ	streamfunction
ω	under-relaxation parameter

Subscripts

c	cold wall or roll centre
e	extrapolated
f	melting or freezing
h	hot wall

int	interface
L	liquidus
max	maximum over cavity
min	minimum over cavity
ref	reference value at T_f
S	solidus
var	variation during one time step

Superscripts

h	energy equation
k	outer iteration index

ACKNOWLEDGEMENTS

Access to the Compaq AlphaServerSC computer was provided by the Center for Computational Sciences at Oak Ridge National Laboratory, which is supported by the Office of Science, U.S. Department of Energy, under Contract No. DE-AC05-00OR22725. The U.S. Government retains a nonexclusive, royalty-free license to publish or reproduce the published form of this contribution, or allow others to do so, for U.S. Government purposes.

Access to the Cray SV1 supercomputer was provided by the Alabama Supercomputer Authority which provides supercomputing time free of charge to faculty and students of the state funded schools of Alabama.

REFERENCES

1. Gau C, Viskanta R. Melting and solidification of a pure metal from a vertical wall. *Journal of Heat Transfer* 1986; **108**:171–174.
2. Brent AD, Voller VR, Reid KJ. Enthalpy-porosity technique for modeling convection–diffusion phase change: application to the melting of a pure metal. *Numerical Heat Transfer* 1988; **13**:297–318.
3. Cruchaga MA, Celentano DJ. A fixed-mesh finite element thermally coupled flow formulation for the numerical analysis of melting processes. *International Journal for Numerical Methods in Engineering* 2001; **51**: 1231–1258.
4. Kim S, Anghaie S, Chen G. A fixed-grid two-phase numerical model for convection-dominated melting and solidification. *Proceedings of the First MIT Conference on Computational Fluid and Solid Mechanics*. MIT: Cambridge, 12–14 June 2001.
5. Lacroix M, Garon A. Numerical solution of phase change problems: and Eulerian–Lagrangian approach. *Numerical Heat Transfer Part B—Fundamentals* 1992; **19**:57–78.
6. Sampath R, Zabaras N. An object oriented implementation of a front tracking finite element method for directional solidification processes. *International Journal for Numerical Methods in Engineering* 1999; **44**:1227–1265.
7. Shyy W, Pal S, Udaykumar HS, Choi D. Structured moving grid and geometric conservation laws for fluid flow computation. *Numerical Heat Transfer Part A—Applications* 1998; **34**:369–397.
8. Viswanath R, Jaluria Y. A comparison of different solution methodologies for melting and solidification problems in enclosures. *Numerical Heat Transfer* 1993; **24**:77–105.
9. Webb BW, Viskanta R. Analysis of heat transfer during melting of a pure metal from an isothermal vertical wall. *Numerical Heat Transfer* 1986; **9**:539–558.
10. Wintruff I, Günther C, Class AG. An interface-tracking control-volume finite-element method for melting and solidification problems—part II: verification and application. *Numerical Heat Transfer Part B—Fundamentals* 2001; **39**:127–149.
11. Roache PJ. *Verification and Validation in Computational Science and Engineering*. Hermosa Publishers: Albuquerque, NM, 1998.
12. Shyy W, Rao MM. Enthalpy based formulation for phase change problems with application to g-Jitter. *Microgravity Science and Technology* 1994; **VII**(1):41–49.

13. Dantzig JA. Modelling liquid–solid phase changes with melt convection. *International Journal for Numerical Methods in Engineering* 1989; **28**:1769–1785.
14. Gobin D, Lequere P. Melting from an isothermal vertical wall: synthesis of a numerical comparison exercise. *Computer Assisted Mechanical Engineering Science* 2000; **7**:289–306.
15. Stella F, Giangi M. Melting of a pure metal on a vertical wall: numerical simulation. *Numerical Heat Transfer Part A—Applications* 2000; **138**:193–208.
16. Hannoun N, Alexiades V, Mai TZ. Resolving the controversy of gallium and tin melting in a rectangular cavity heated from the side. *Numerical Heat Transfer Part A—Applications* 2003; **44**(3):253–276.
17. Bertrand O, Binet B, Combeau H, Couturier S, Delannoy Y, Gobin D, Lacroix M, Lequere P, Medale M, Mencinger J, Sadat H, Vieira G. Melting driven by natural convection. A comparison exercise: first results. *International Journal of Thermal Sciences* 1999; **38**:5–26.
18. Mencinger J. Numerical simulation of melting in two-dimensional cavity using adaptive grid. *Journal of Computational Physics* 2004; **198**:243–264.
19. Alexiades V, Solomon AD. *Mathematical Modeling of Melting and Freezing Processes*. Hemisphere: Washington, DC, 1993.
20. Shamsunder N, Sparrow EM. Analysis of multidimensional phase change via the enthalpy model. *Journal of Heat Transfer* 1975; **98**:333–340.
21. Patankar SV. Elliptic systems: finite-difference method I. *Handbook of Numerical Heat Transfer*. Wiley: New York, 1988.
22. Ghia U, Ghia KN, Shin T. High-Re solutions for incompressible flow using the Navier–Stokes equations and a multigrid method. *Journal of Computational Physics* 1982; **48**:387–411.
23. Hortman M, Peric M, Sheuerer G. Finite volume multigrid prediction of laminar natural convection: benchmark solutions. *International Journal for Numerical Methods in Fluids* 1990; **11**:189–207.
24. Shyy W, Udaykumar HS, Rao MM, Smith RW. *Computational Fluid Dynamics with Moving Boundaries*. Taylor and Francis: London, 1995.
25. Juric D, Tryggvason G. A front tracking method for dentritic solidification. *Journal of Computational Physics* 1996; **123**:127–148.
26. Udyakumar HS, Mittal R, Shyy W. Computation of solid–liquid phase fronts in the sharp interface limit on fixed grids. *Journal of Computational Physics* 1999; **154**:468–496.
27. Beckermann C, Diepers HJ, Steinbach I, Karma A, Tong X. Modeling melt convection in phase-field simulations of solidification. *Journal of Computational Physics* 1999; **153**:535–574.
28. Lacroix M, Voller VR. Finite difference solutions of solidification phase change problems: transformed versus fixed grids. *Numerical Heat Transfer Part B—Fundamentals* 1990; **17**:25–41.

